Research article

Deciphering the role of ferroptosis in rheumatoid arthritis: Synovial transcriptome analysis and immune infiltration correlation

Hongli Wang [a,b], Miaomiao Zhang [a,b], Yiping Hu [a,b], Juan He [a,b], Yuchao Zhong [a,b], Yong Dai [a,b,**], Qingwen Wang [a,b,*]

[a] *Department of Rheumatism and Immunology, Peking University Shenzhen Hospital, Shenzhen, China*
[b] *The Key Laboratory of Inflammatory and Immunology Diseases, Shenzhen, China*

A B S T R A C T

The pathogenesis of rheumatoid arthritis (RA) remains elusive. The initiation of joint degeneration is characterized by the loss of self-tolerance in peripheral joints. Ferroptosis, a form of regulated cell death, holds significant importance in the pathophysiology of inflammatory arthritis, primarily due to iron accumulation and the subsequent lipid peroxidation.

The present study investigated the association between synovial lesions and ferroptosis-related genes using previously published data from rheumatoid patients. Transcriptome differential gene analysis was employed to identify ferroptosis-related differentially expressed genes (FRDEGs). To validate FRDEGs and screen hub genes, we used weighted gene co-expression network analysis (WGCNA) and receiver operating characteristic (ROC) curves. Subsequently, immune infiltration analysis and single cell analysis were conducted to investigate the relationship between various synovial tissues cells and FRDEGs. The findings were further confirmed through reverse transcription-quantitative polymerase chain reaction (RT-qPCR), immunohistochemical staining, and immunofluorescence techniques.

Upon intersecting DEGs with ferroptosis-related genes, we identified a total of 104 FRDEGs. Through the construction of a protein-protein interaction (PPI) network, we pinpointed the top 20 most highly concentrated genes as hub genes. Subsequent analyses using ROC curve and WGCNA validated eight FRDEGs: TIMP1, JUN, EGFR, SREBF1, ADIPOQ, SCD, AR, and FABP4. Immuno-infiltration analyses revealed significant infiltration of immune cell in RA synovial tissues and their correlations with the FRDEGs. Notably, TIMP1 demonstrated a positive correlation with various immune cell populations. Single-cell sequencing date of RA synovial tissue revealed predominant expression of TIMP1 is in fibroblasts. RT–qPCR, immunohistochemistry, and immunofluorescence analyses confirmed significant upregulation of TIMP1 at both mRNA and protein levels in RA synovial tissues and fibroblast-like synoviocytes (FLS).

The findings provide novel insights into pathophysiology of peripheral immune tolerance deficiency in RA. The dysregulation of TIMP1, a gene associated with ferroptosis, was significantly observed in RA patients, suggesting its potential as a promising biomarker and therapeutic target.

* Corresponding author. Department of Rheumatism and Immunology, Peking University Shenzhen Hospital, No.1120, Lianhua Road, Futian District, Shenzhen 518036, China.
** Corresponding author.
E-mail addresses: daiyong22@aliyun.com (Y. Dai), wqw_sw@163.com (Q. Wang).

1. Introduction

Rheumatoid arthritis (RA) is a chronic and heterogeneous autoimmune disease that has the potential to affect multiple systemic organs. It is characterized by inflammatory infiltration of the synovium and joints, as well as the presence of autoantibodies such as anti-citrullinated protein antibodies (ACPAs) and rheumatoid factor (RF). The precise pathogenesis of RA remains incompletely understood. However, it is associated with a decrease in T cell tolerance, the gradual emergence of tissue-invasive effector T cell populations, and the transition from normal fibroblasts to tissue-destructive fibroblasts within the affected joints [1]. The prevalence of RA varies among different ethnicities, typically ranging from 0.5 % to 1.0 % [2]. A recently proposed model for interpreting autoimmunity suggests that organ dysfunction occurs due to imbalanced autoimmunity states, leading to inhibition, destruction, and/or atrophy of cells. RA can be classified into two phases: preclinical RA and established RA based on pathogenic autoimmunity [3]. During the onset of RA, there are three crucial immune checkpoints that signify the transition from asymptomatic autoimmune anomalies to irreversible joint damage: the breakdown of self-tolerance in the immune system, the loss of self-tolerance in tissues, and the progression from acute to chronic synovitis [4]. The presence of each checkpoint triggers a decline in tolerance, leading to a shift in physiological immune system towards pathogenic immunity. This perpetuates and exacerbates the pathological manifestations of RA. Ferroptosis represents a distinct form of regulated cell death triggered by disruptions in iron metabolism and lipid peroxidation [5]. In contrast to conventional apoptosis, characteristics of ferroptosis include a notable reduction in mitochondrial volume, diminished or absent mitochondrial cristae, an elevation in mitochondrial membrane density, and compromise of the mitochondrial outer membrane (MOM) [6]. Beyond these mitochondrial alterations, lipid peroxidation also induces the disruption of cellular membranes [6]. Cytoplasmic divalent ferrous ions (Fe^{2+}) facilitate the generation of reactive oxygen species (ROS) by catalyzing lipid peroxidation, either through lipoxygenase activity or the Fenton reaction [7]. The interplay between ROS and PUFAs triggers lipid peroxidation in the context of ferroptosis, leading to the dysfunction of membrane enzymes and ultimately altering the permeability and fluidity of the plasma membrane [8].

As early as 1968, scientists observed an accumulation of iron in the synovial tissues of RA patients [9]. Subsequent investigations consistently revealed that pro-inflammatory cytokines induce FLS and monocytes in RA patients to uptake iron and there is a positive correlation between iron overload and disease activity [10,11]. The involvement of reactive of ROS in the pathogenesis of RA is significant. Specifically, ROS activate matrix metalloproteinases (MMPs), which not only inhibit cartilage synthesis but also promote FLS proliferation and chondrocyte apoptosis in RA [12]. It is worth noting that patients with RA exhibit markedly elevated concentrations of lipid peroxidation products [13].

The mitochondria function as the primary locus of ferroptosis, playing a crucial role in the generation of mitochondrial ROS (mitoROS). In individuals with RA, the mitoROS levels in peripheral blood are quintuple those observed in healthy subjects [14].
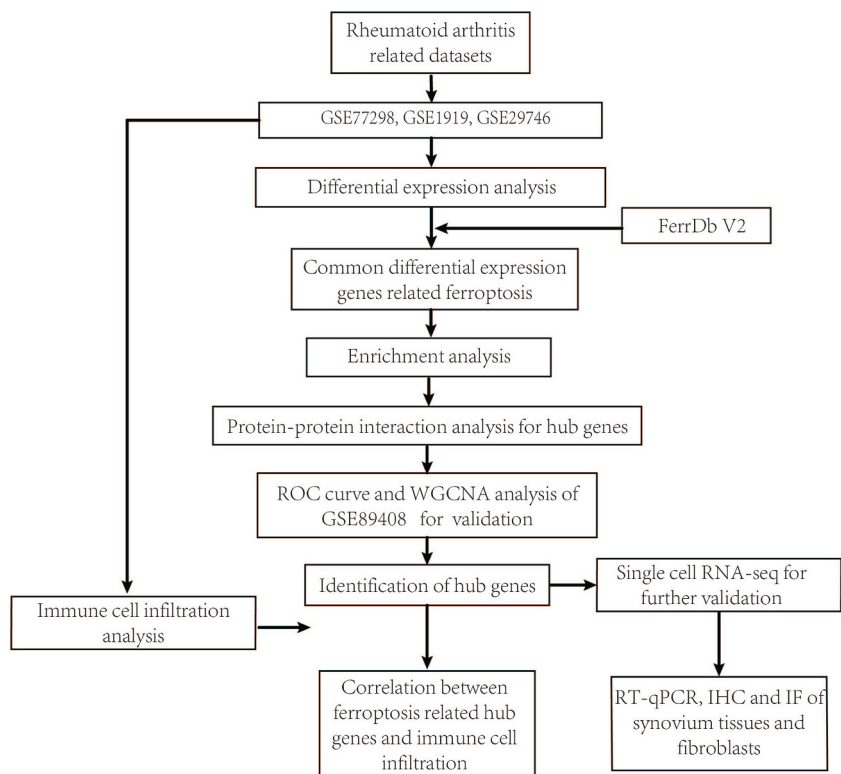

Fig. 1. Flowchart of the study workflow.

Additionally, mitochondrial dysfunction is frequently observed in RA-afflicted FLS [15].

In summary, ferroptosis expedited the onset and exacerbation of RA. However, the precise signaling pathways and functions underlying ferroptosis in the pathogenesis and progression of RA remains elusive. Consequently, investigating the potential pathways by which ferroptosis induce cell death in RA synovial tissues might unveil innovative therapeutic strategies for RA management.

Bioinformatics, empowered by advancements in transcriptomics and single-cell technologies, has emerged as a potent tool for identifying biomarkers and comprehending molecular mechanisms underlying autoimmune diseases. This study employed bioinformatics technology to pinpoint differentially expressed genes (DEGs) linked to ferroptosis in RA synovial tissues, elucidated the biological function and signaling pathways they engage in, and delved into the interplay between ferroptosis and immune dysregulation. The methodology of the study is delineated in Fig. 1.

2. Materials and methods

2.1. Dataset acquisition

Microarray expression data for GSE77298, GSE1919, and GSE206848 were obtained from the Gene Expression Omnibus (GEO) database (https://www.ncbi.nlm.nih.gov/geo; accessed on February 18, 2023). The specifics of the datasets and samples are provided in Table 1. Each sample contained either synovial tissues or synovial fluids. Probes within datasets were annotated and standardized using the GEO platform (GPL). When a single gene was represented by multiple probes, the average value was utilized denote its expression level.

2.2. Differentially expressed genes (DEGs) analysis

To screen DEGs between RA and normal controls tissues, the limma package [16] in R (version 4.0.5, Auckland, New Zealand) was used. The standards for filtering were adj.p-value <0.05 and $|log2FC| \geq 0.80$ (fold change).

2.3. Ferroptosis-related DEGs (FRDEGs) acquisition

FerrDb is a manual database [17] of biomarkers associated with ferroptosis derived from published journal papers. Data for FRDEGs were procured using the FerrDb (accessed on February 18, 2023, http://www.zhounan.org/ferrdb) and then analyzed by intersecting with the DEGs. The online web tool-Jvenn (http://jvenn.toulouse.inra.fr/app/example.html) [18] was used for visualization.

2.4. Biological functional and pathway enrichment analysis

We employed DAVID 6.8 (https://david.ncifcrf.gov/home.jsp; obtained on February 18, 2023), a comprehensive gene annotation tool proficient in Gene Ontology (GO) and Kyoto Encyclopedia of Genes and Genomes (KEGG) pathway enrichment analysis, to elucidate the functions and signaling pathways of FRDEGs dentified by the previously mentioned approach. A false discovery rate (FDR) values of <0.05 was set as the threshold to determine the significance of functions and pathways.

2.5. Protein–protein interaction (PPI) network construction

The STRING database (http://string-db.org, accessed on February 18, 2023) was harnessed to construct the PPI network for FRDEGs. The PPI network was visualizedusing Cytoscape (Version 3.9.1, San Diego, CA, United States). Hub genes were then identified from the most prominent module within the network, utilizing the CytoHubba plugin (Version 0.1). Utilizing the CytoHubba plugin, we adopted the Maximal Clique Centrality (MCC) algorithm to identify critical proteins within the network. By integrating connectivity and MCC scores, we selected the top 20 proteins in the network as key proteins. 2.6 Identification and Validation of Optimum Hub FRDEGs.

To identify the most significant hub FRDEGs, we conducted validation using the GSE89408 dataset, focusing on the top 20 genes. Receiver operating characteristic (ROC) curves were employed to validate the levels of hub FRDEGs that distinguish individuals with (RA from control groups were validated, along with, assessing their diagnostic value. We created a model using the roc function in the pROC package (version 1.18.5), found the optimal cutoff point with the coords function, and calculated the AUC value using the auc

Table 1
The detailed characteristics of the datasets.

Dataset	Platform	Tissue	Species	Type	Number of samples (RA/CN)
GSE77298	GPL570	Synovial tissues	Homo sapiens	mRNA	16/7
GSE1919	GPL91	Synovial tissues	Homo sapiens	mRNA	5/5
GSE29746	GPL4133	Synovial fluid	Homo sapiens	mRNA	9/11
GSE89408	GPL11154	Synovial tissues	Homo sapiens	mRNA	152/28

RA/CN: Rheumatoid arthritis patients and controls.

function.

2.7 Co-expression Genic Network Construction Weighted gene co-expression network analysis (WGCNA) is a widely-utilized bioinformatics algorithm for exploringgene-phenotype relationships [19]. The GSE89408 dataset matrix served as the basis for constructing the WGCNA using R A set of genes with absolute deviations of exceeding 25 % from the median was chosen for analysis, using WGCNA package (1.72-1). The "goodSampleGenes" function was utilized to validate data integrity. The "PickSoftThreshold" function was utilized to determine and validate the optimal soft threshold. The matrix was then transformed into an adjacency matrix, and modules were identified based on topological overlap through clustering with the unsigned TOM/network. Subsequently, module eigengene (ME) calculations and the merging of correlated modules based on ME were conducted. Clustering dendrograms were generated. We assessed the significance of genes and clinical information using modules and phenotypic data, as well as examined the associations between models and FRDEGs. We also examined the expression of FRDEGs in meaningful modules identified by WGCNA within the GSE89408 dataset.

2.6. Immune cell infiltration analysis

To confirm immune cell infiltration and mitigate algorithm discrepancies, we estimated immune cell proportions in synovial tissues of RA patients through gene expression analysis (GSE89408 and GSE1919) utilizing xCell (https://xcell.ucsf.edu, version = 1.1.0) [20]. In the xCell analysis, we first utilized the rawEnrichmentAnalysis to calculate enrichment scores, followed by normalization using the transformScores function. The spillOver function was then applied to adjust scores using the spillover compensation method. Finally, the xCellAnalysis function was used to return the xCell cell types enrichment scores, using default parameters. Visualization was performed using pheatmap, ComplexHeatmap, and ggplot2.

Using R (version 4.0.5, Auckland, New Zealand), the Pearson's correlation coefficient between FRDEGs and the proportion of immune cells was computed.

2.7. Single-cell RNA-sequencing (scRNA-seq) for further investigation

scRNA-Seq data are available at ImmPort (https://www.immport.org/shared/study, code SDY998). Following the standard procedure for Seurat single-cell analysis [21,22], the dataset underwent preprocessing to generate a Seurat. Low-quality cells, defined as those with >15 % mitochondrial genes and <200 measured genes, were excluded. Following filtration 6186 cells remained for subsequent analyses. The Seurat was normalized ("LogNormalize," with a scale factor of 10,000), and the 2500 most variable genes were elected and scaled. For UMAP visualization, the top 13 principal components were used, and clustering was performed with a resolution of0.1. All procedures were executed using functions from the Harmony and Seurat packages ("NormalizeData", "FindVariableFeatures", "ScaleData", "RunPCA", "FindNeighbours", "FindClusters", "RunUMAP").

Canonical marker genes, such as PDGFRA, ISLR, THY1 (fibroblasts) CD3D, CD2 (CD4$^+$ T cells); CD8A (CD8$^+$ T cells); CD79A, CD37, XBP1 (B cells); CD38 (plasmablasts); and CD14, C1QA (monocytes) were employed to characterize cell types, as showed in Fig. 9B.

2.8. Patients

Synovial biopsies were obtained from three patients with RA and three RA-free controls underwent knee surgery. We also preserved synovial tissues from three RA patients and three controls without rheumatic diseases. Primary FLS was obtained for subsequent experiments [23]. All subjects provided written permission. The investigation was approved by the Shenzhen Hospital of Peking University and conducted in accordance with their accredited ethical guidelines (2020–007). FLS were nurtured in Dulbecco's modified Eagle medium (DMEM), 10 % fetal bovine serum (Gibco, USA) in a 37 °C, 5 % carbon dioxide incubator. The main FLS used in this study were passages 1 through 4.

2.9. Reverse transcription–quantitative polymerase chain reaction (RT–qPCR)

Total RNA was extracted from synovial tissues using TRIzol reagent (Thermo Fisher, MA, USA) following manual tissue grinding. Reverse-transcription to cDNA was performed using the appropriate reagents. The resulting cDNA was utilized as templates for RT–qPCR; the TIMP1 primer sequence was as follows: F: 5′-CACTGTTGGCTGAGGAATGC-3′; R: 5′-GAGGCAGGCAAGGTG-3′. GAPDH was used as the reference gene. The 2-ΔΔCt method was applied to calculate the relative expression of mRNA [24]. The expression of TIMP1 in the control group was determined to be 1.

2.10. Immunohistochemistry

Immunohistochemical staining of TIMP1 was conducted. After deparaffinization, rehydration, and washing, sections were antigen-retrieved using pepsin and cultured for 10 min with 0.3 % hydrogen peroxide to impede endogenous peroxidase. To prevent nonspecific background staining, a protein block was incubated for 10 min at room temperature. The sections were incubated with anti-TIMP1 antibody (Abcam, Cambridge, MA, ab211926) at a dilution of 1:1000. The sections were then treated according to the manufacturer's instructions (Origene, pv-6001) with biotinylated secondary antibody and color development. Using the Image-Pro plus 6.0 software, the mean optical density (MOD) was calculated in order to analyze the semi-quantitative expression of TIMP1. Two sections were chosen at random for each vision from six distinct regions on each stained section. Each group contained 12

samples.2.13 Immunofluorescence.

Cells were cultivated for 24 h in 96-well culture plates (6000 cells per well) for protein staining. After that, the FLS were fixed 15 min with 0.1 % Triton X-100. Then, cells were incubated with 1.5 % bovine serum albumin (Merck, Germany) at room temperature (RT) for 45 min. FLS were incubated for 30 min at RT with rabbit anti-TIMP1 antibody (Abcam, Cambridge, MA, ab211926). The cells were then probed with an Alexa Fluor 488-labeled immunoglobulin G antibody (A-11008, Invitrogen, USA) and then incubated for 30 min at RT with 4′,6-diamidino-2-phenylindole (AAT Bioquest, USA). A fluorescent microscope was used to capture FLS images.2.14 Statistical Analysis.

Quantitative data were displayed as the mean ± standard deviation (SD). Statistical significance was determined using the T-test for paired samples. p-values of <0.05 or <0.01 were considered statistically significant. All statistical analyses were calculated and visualized using GraphPad Prism 8.0 for Windows.
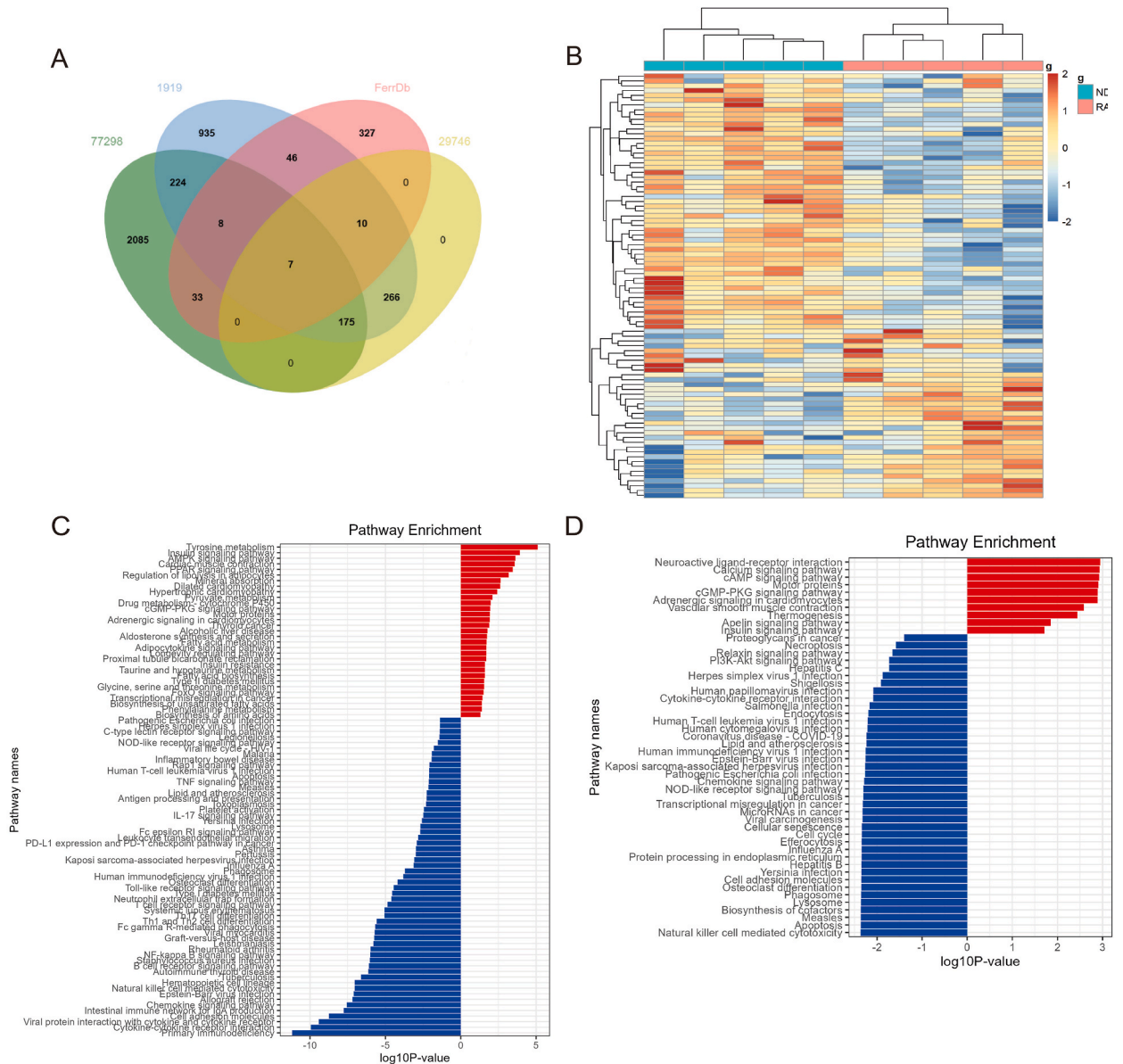

Fig. 2. A Obtained and screened FRDEGs (n = 104); B Expression of FRDEGs visualized via a cluster heatmap of GSE29746C, the horizontal axis demonstrates that samples from the RA group and the NC group are well-clustered; C,D The KEGG analysis results of DEGs from the GSE77298 and GSE1919 datasets. FREDGs: ferroptosis-related differentially expressed genes; KEGG: Kyoto Encyclopedia of Genes and Genomes.

3. Results

3.1. Identification of ferroptosis-related differentially expressed genes inRA

In this study, we retrospectively analyzed data from 30 RA samples and 23 control samples from GSE77298, GSE1919, and GSE29746 to pinpoint potential FRDEGs associated with RA. Upon establishing an interaction between DEGs and ferroptosis genes, we identified 104 FRDEGs,as presented in Fig. 2A, the gene list appling in supplementary Material 1. The expression of FRDEGs depicted as a clustered heatmap showed significant differences between the RA and normal populations (Fig. 2B).

3.2. Enrichment analysis of FRDEGs and synovial tissues of RA

We used KEGG analyses to discern the biological processes and signaling pathways linked to FRDEGs. KEGG revealed that FRDEGs were primarily enriched in the JAK–STAT signaling pathway, NOD-like receptor signaling pathway, PPAR signaling pathway, lipid and atherosclerosis, HIF-1 signaling pathway and ferroptosis. (Supplemental Fig. 1). These findings suggest that the identified FRDEGs are likely to be extensively involved in the pathogenesis of RA synovium through these signaling pathways. Concurrently, enrichment analysis of the synovium transcriptome's DEGs identified pathways such as the PPAR signaling pathway, lipid metabolism-related pathways, and the cAMP signaling pathway, as shown in Fig. 2C and D. Given the known extensive involvement of the ferroptosis pathway in pathophysiological processes such as lipid metabolism, mitochondrial dysfunction, and oxidative stress, the enrichment analysis results of these FRDEGs provide us with clues to investigate the potential pathogenic pathways of ferroptosis in RA synovium, such as the PPAR signaling pathway.

3.3. Determination and validation of hub FRDEGs

The FRDEGs were subjected to PPI network analysis using the STRING web tool and Cytoscape to investigate their relationships and identify key genes in the network. The presence of a node with a higher degree, indicating an increased number of edges, implies its potential to exert significant influence on the network (Fig. 3A). The top 20 hub FRDEGs were obtained by the CytoHubba plugin (Fig. 3B). To assess the diagnostic potential of the top 20 hub genes in RA patients, we conducted ROC curves using the GSE89408 dataset. The area under the curve (AUC) values for 13 of these genes (JUN, EGFR, CCND1, CD44, PTGS2, TIMP1, AR, SREBF1, ADIPOQ, SCD, PLIN2, FABP4, and EGR1) exceeded 0.70 (Fig. 4). The findings imply that these genes have the potential to function as discerning biomarkers for RA to a certain extent.

The goal of WGCNA is to identify clusters of co-expressed genes within large gene datasets. It categorizes genes into modules and identifies potential biomarker genes based on the interconnectivity within the gene set and its association with phenotypic traits. By applying WGCNA, we can validate FRDEGs from another algorithmic perspective.

Using the WGCNA, we successfully identified a total 11 modules in the GSE89408 dataset by selecting an optimal soft threshold of 8 (Supplemental Fig. 2). To evaluate the association between each module and the disease, we employed a heatmap to visualize the module-trait relationships based on the Spearman correlation coefficient (Fig. 5B). The brown module (r = 0.55, p = 2e15), blue module (r = −0.67, p = 1e24), green module (r = 0.46, p = 6e11), and turquoise module (r = 0.73, p = 3e31) demonstrated significant correlations with RA. The turquoise module contained JUN, EGFR, and SREBF1; the green module contained ADIPOQ, SCD, AR, and FABP4; the brown module contained TIMP1.Further analysis involved GO enrichment analysis for each module, with the turquoise
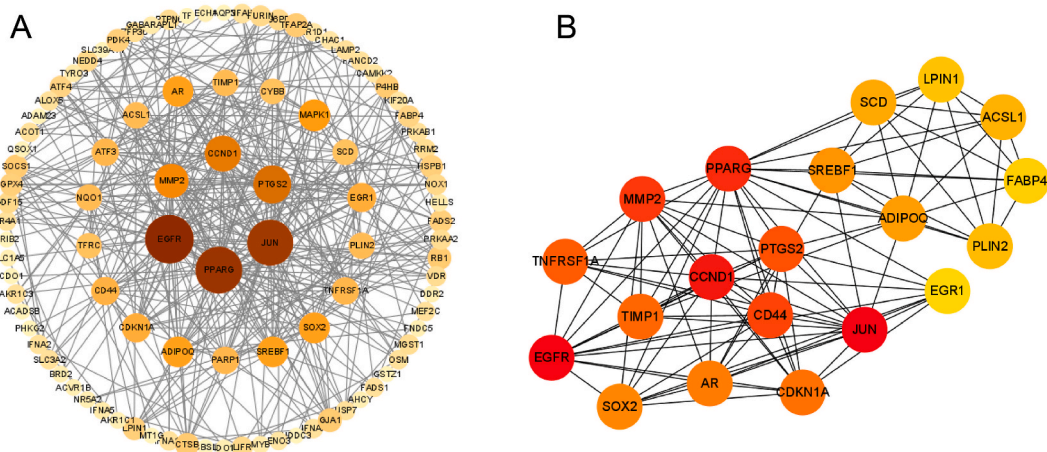

Fig. 3. PPI network of FRDEGs. A FRDEGs applied to PPI analysis, darker colors and larger points indicating higher degree; B 20 hub FRDEGs obtained according to the MCC algorithm of the CytoHubba plugin. (For interpretation of the references to color in this figure legend, the reader is referred to the Web version of this article.)
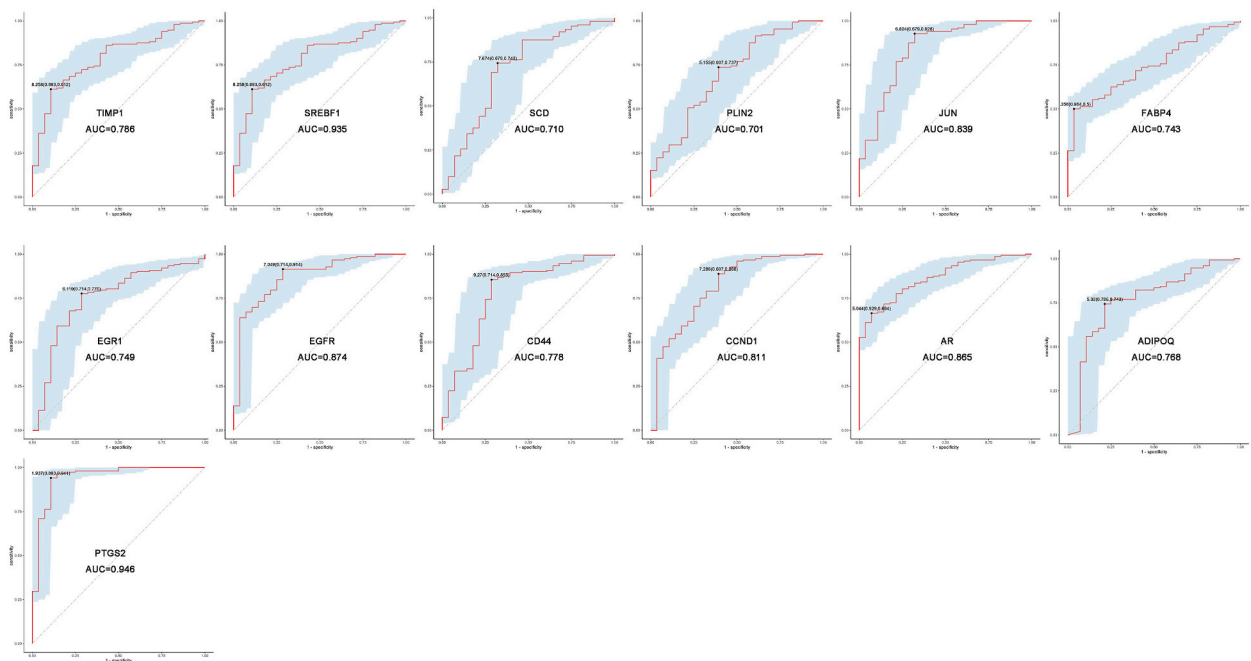
Fig. 4. ROC analysis for further validation of hub FRDEGs using GSE89408 dataset. The results showing AUC values of 13 genes for which FRDEGs were highly indicative of RA. ROC: Receiver Operating Characteristic Curve; AUC: area under the curve.

module showing enrichment in entries such as oxidoreduction-driven activity and NADPH dehydrogenase activity, while the brown module was enriched in entries including cytokine activity, SH2 domain binding, and lipopeptide binding (Fig. 5C). These modules are intricately associated with the clinical phenotype and encompass FRDEGs. The association further emphasizes, through multiple analytical approaches, that these FRDEGs are likely contributors to the abnormal pathophysiology observed in the RA synovium. This was also verified in the GSE89408 dataset, where it was found that the mRNA levels of TIMP1 were significantly increased in RA tissues (Fig. 6).

3.4. The infiltration of immune in the synovium of RA and its association with eight FRDEGs

In order to gain a comprehensive understanding of immune cell infiltration in the synovium of patients with rheumatoid arthritis and its correlation with the identified FRDEGs, we analyzed datasets GSE1919 and GSE89408. Notably, the synovium of the RA group exhibited increased lymphocyte scores, encompassing various subsets including naïve $CD4^+$ T cells, memory $CD4^+$ T cells, effector memory $CD4^+$ T cells (Tem), $CD8^+$ T cells, central memory $CD8^+$ T cells (Tcm), $CD8^+$ Tems, T helper 2 (Th2) cells, naive B cells, memory B cells, and plasma cells (Fig. 7A and B). Conversely, a decline in $CD4^+$ Tcms was observed in RA synovium tissues. Furthermore, the infiltration scores for monocytes, dendritic cells, M0 macrophages, and M1 macrophages in the RA synovial tissues were notably elevated in comparison to control samples (Fig. 7A and B). The correlation between infiltrated immune cell infiltrations is further elucidated in Fig. 8A. Upon conducting a gene-immune cell correlation analysis, (Fig. 8B), we ascertained that the expressions of TIMP1, EGFR, FABP4, ADIPOQ, and JUN were strongly correlated with the activation of macrophages and $CD8^+$ T cells, whereas TIMP1 and FABP4 were strongly correlated with B cells. Collectively, these observations underscore that the expression patterns of the afore mentioned FRDEGs might modulate immune cell activity. TIMP1 demonstrates a significant positive correlation with various immune cells, suggesting its potential involvement in the peripheral arthropathy observed in RA.

3.5. scRNA-seq reveals Intercellular expression differences of FRDEGs in RA synovium

In our study, we examined both microarray data and traditional high-throughput sequencing data, employing diverse analytical methods to identify FRDEGs. It is important to note that peripheral synoviocytes in RA comprise multiple cellular components. To better understand the expression of FRDEGs across these cell types in RA synovial tissues, we analyzed a scRNA-seq dataset from RA-affected joint synovial tissues. By utilizing dimensionality reduction techniques on the single-cell data and subsequently annotating the cell subpopulations, we observed the expression patterns of FRDEG across different cell population. This approach also facilitated a more comprehensive understanding of immune cell infiltration within the synovial tissues.

A total of 6186 cells were obtained and subjected to dimensionality reduction. Subsequent unsupervised clustering of these cells yielded 13 distinct clusters. Based on canonical marker genes, we identified nine cell type, as depicted in Fig. 9A: B cells, $CD8^+$ T cells, $CD4^+$ T cells, fibroblasts, monocytes and plasmablasts. Figure. We explored the expression of JUN, EGFR, SREBF1, ADIPOQ, SCD, AR,
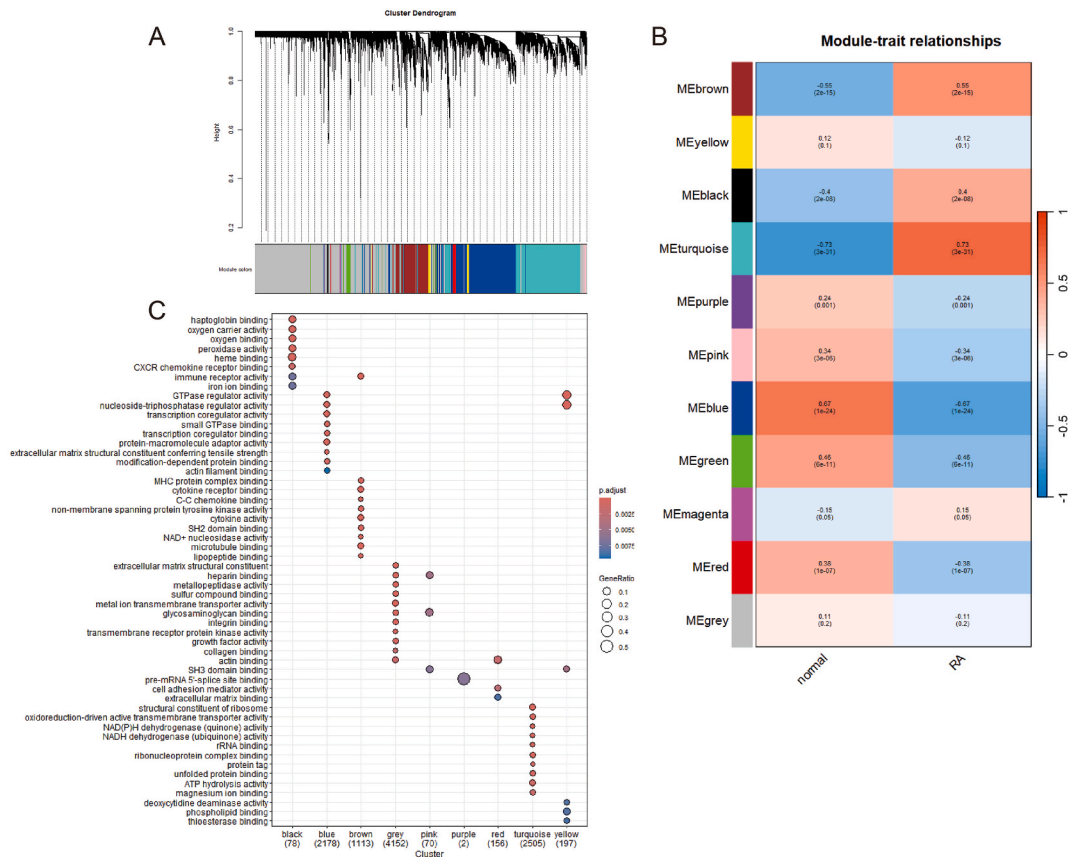
Fig. 5. The WGCNA analysis of the GSE89408 dataset. A The hierarchical cluster tree of the WGCNA , showing the modules of co-expressed genes; B The correlation of each module with RA, where redder colors indicate higher positive correlation and darker colors indicate higher negative correlation; C The results of the GO enrichment analysis for the genes in each module. (For interpretation of the references to color in this figure legend, the reader is referred to the Web version of this article.)
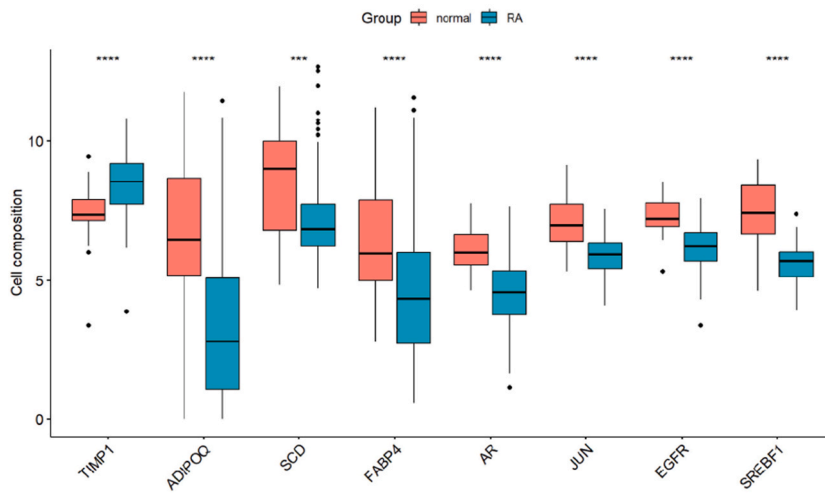
Fig. 6. Eight hub FRDEGs regulated in synovium tissues between RA and normal control samples in the GSE89408 dataset. Except for TIMP1, which is upregulated in RA, other genes are expressed at higher levels in the normal group.
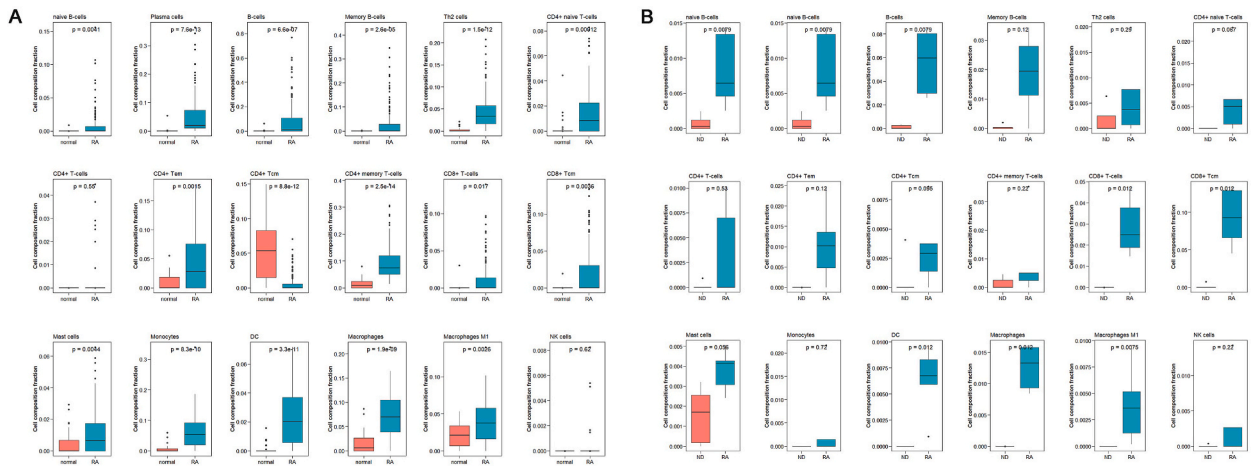
Fig. 7. Boxplots of immune cells for the GSE89408 and GSE1919dataset via the xcell algorithm. Utilizing the xCell algorithm to explore the infiltration of 64 types of immune cells in synovial tissues. The figure illustrates the infiltration of certain immune cells within datasets GSE89408(A) and GSE1919 (B).
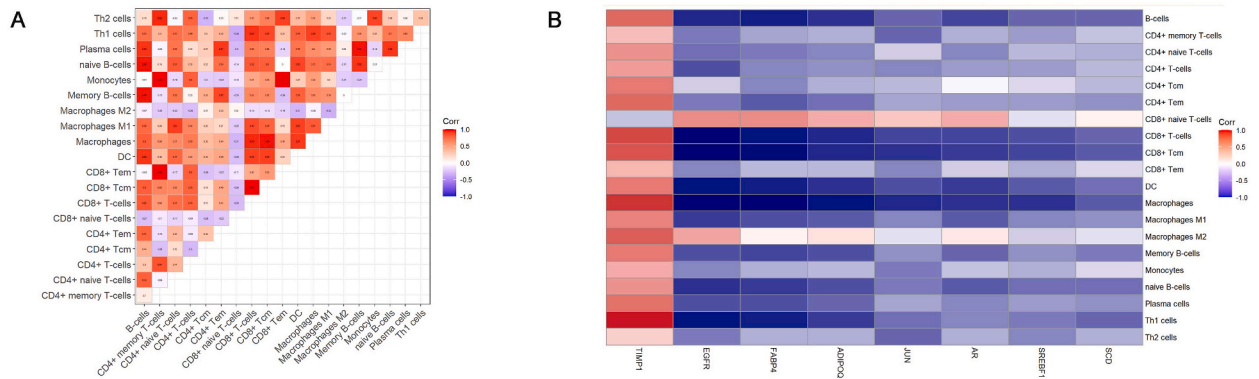

Fig. 8. Immune cell infiltration in the GSE1919 dataset. A Identification of immune cells with notably different infiltration patterns and the correlations among infiltrating immune cells; B The correlation between 8 hub FRDEGs and infiltrating immune cells, showing that TIMP1 has a significant positive correlation with many pro-inflammatory immune cells.

FABP4, and TIMP1 in various cell types and found that TIMP1, JUN, EGFR, SREBF1, and LRP1 are highly expressed in various cells of the synovial tissue. Notably, TIMP1 and LRP1 were found to be specifically overexpressed in fibroblasts (Fig. 10).

As previously reported , the metalloproteinase inhibitor TIMP1 plays a crucial role in the degradation of the extracellular matrix [25], which is closely associated with RA and its joint destruction. Consequently, this discovery has prompted further conventional experimental validation.

3.6. TIMP1 is significantly upregulated in both synovial tissues and FLS of RA

We observed a prominent upregulation of TIMP1 in both the synovial tissues and synovial fibroblasts derived from RA patients. To further validat, this upregulation was confirmed at both the mRNA and protein levels. RT–qPCR analysis reveals a significant increase in TIMP1 mRNA expression in synovial tissues and FLS, as presented in Figs. 11A and 12A. Moreover, in the fracture synovial regions of RA patients, the expression levels of TIMP1 protein were significantly higher in the RA group compared to the control group (p < 0.01; Fig. 11B and C). In tandem with this, immunofluorescence staining of FLS highlighted a stronger fluorescence intensity associated with the target protein in RA compared to the control (p < 0.01; Fig. 12B and C).

4. Discussion

RA, one of most prevalent autoimmune diseases, primarily affects the synovial tissues in joints, leading to chronic inflammation, joint deterioration, and potential disability [4]. While some studies have suggested a possible association between ferroptosis and the development of inflammatory arthritis [14], the precise relationship between ferroptosis and peripheral arthropathy in RA,
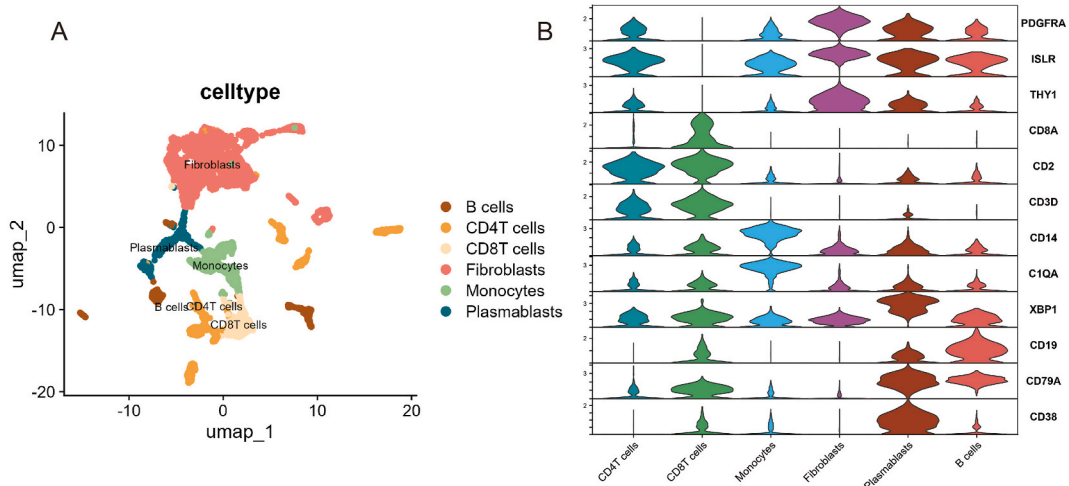
Fig. 9. scRNA-seq analysis of the synovial tissues of RA. A Clustering of all cells, UMAP plots denoting five cell types. B "The violin plot represents the expression of characteristic cell marker genes for each cell type UMAP: uniform manifold approximation and projection.
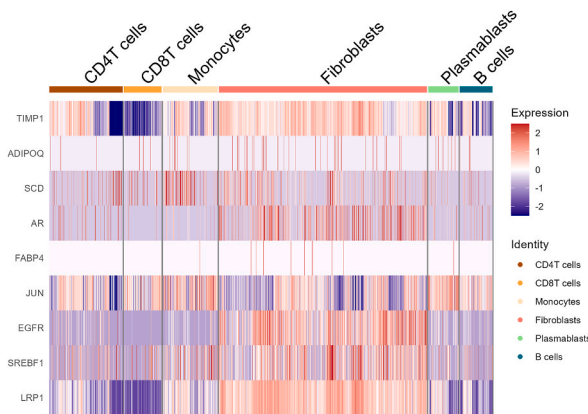

Fig. 10. The heatmap of eight hub FRDEG expressions in clusters of cell types.

particularly within synovial tissues, remains to be elucidated. Therefore, we utilized a combination of bioinformatics analyses to identify potential biomarkers of RA associated with ferroptosis and to investigate new pathogenic mechanisms of synovial lesions in RA.

This study identified 104 DEGs that may be implicated in ferroptosis, based on the analysis of synovial microarray datasets of RA from the GEO database. These FRDEGs are substantially enriched in PPAR signaling pathway, HIF-1 signaling pathway, NOD-like receptor signaling pathway, JAK-STAT signaling pathway, and lipid and atherosclerosis pathways, as determined by KEGG enrichment analysis. These pathways have been demonstrated to be extensively involved in the pathophysiological processes of RA [26]. They may also play a role in the regulation of ferroptosis. For instance, studies have found that MDM2 and MDMX, known for their oncogenic effects, can promote ferroptosis by remodeling lipid metabolism through the PPAR signaling pathway [27].

Numerous studies have discovered an inseparable link between ferroptosis and signaling pathways. The activation of ferroptosis triggers a series of responses, and certain signaling pathways can regulate ferroptosis, including the JAK-STAT, NF-κB, inflammasome, and cGAS-STING signaling pathways [28]. This finding also suggests the possibility of such a phenomenon.

Recent studies have definitively established the involvement of ferroptosis in the RA pathogenesis. Iron load and the protein level of transferrin receptor protein 1 (TfR1) and nuclear receptor coactivator 4(NCOA4) is increased in synovial cells. In the LPS-induced RA model, there is a decline in the expressions of glutathione peroxidase 4 (GPX4), solute carrier family 7 member 11(SLC7A11), and NFE2 Like BZIP transcription factor 2(NRF2), culminating in augmented synovial cell mortality [29]. Multiple studies have confirmed perturbed iron metabolism in RA. In conditions such as hemophilia and hemochromatosis, Van Vulpen et al. determined that excess iron precipitates synovial inflammation and dysplasia, decreased chondrocytes, and dysfunction of osteoblasts, resulting in joint destruction [30]. ROS plays a pivotal role in RA progression, and its regulation is intrinsic to ferroptosis. Lipid peroxidation metabolic alterations in RA has gained momentum in research circles. According to a study, the levels of malondialdehyde (MDA) and glutathione peroxidase (GPx) in blood is elevated in serum, while GSH and GPx levels are decreased, which correlates with disease activity
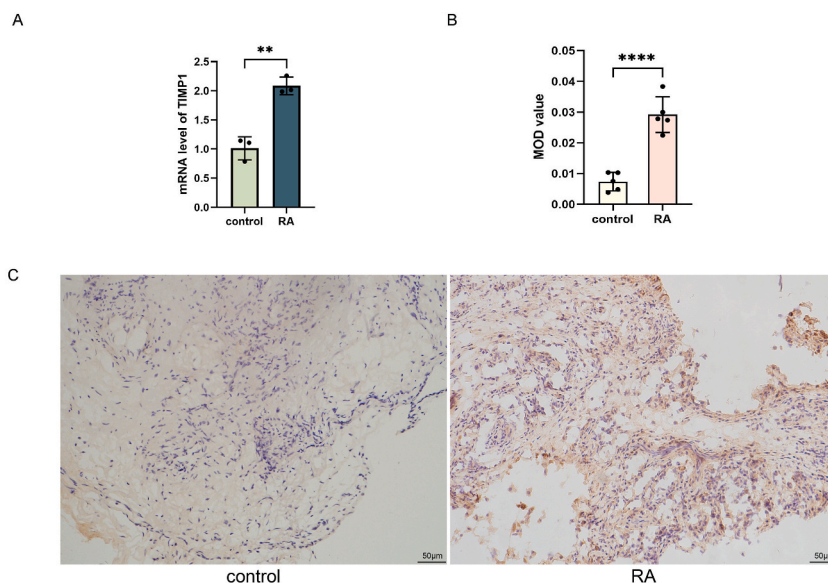
Fig. 11. RT–qPCR and histologic analysis of synovial tissues from RA patients and control groups. (A) RT–qPCR analysis of TIMP1 mRNA in the control and RA groups. (B) Statistical data of mean optical density (MOD) in fracture areas between groups. ****p < 0.01 compared with the control group. (C) Tissue sections were stained with TIMP1 to check the protein expression in RA patients (original magnification × 200).

[31]. In recent discourse, the potential contribution of mitochondrial dysfunction m to RA inflammation has been proposed. Levels of mitoROS of RA patients are quintuple those in healthy individuals, present in both blood and monocytes [14]. The primary progenitors of mitoROS are Oxidative phosphorylation (OXPHOS) complexes in mitochondria. Hence, mitochondrion could represent a pivotal nexus in the intertwined processes of RA and ferroptosis.

In this study, eight FRDEGs (TIMP1, JUN, EGFR, SREBF1, ADIPOQ, SCD, AR, and FABP4) were identified. Importantly, TIMP1 exhibited a significant upregulation in synovial tissues of RA in the validation dataset. Single-cell sequencing of RA synovial tissues revealed a pronounced expression of TIMP1 in fibroblasts and mural cells, with lower expression observed in NK cells and macrophages.

Further validation using RT–qPCR and immunohistochemistry investigations confirmed a trend toward elevated TIMP1 mRNA and protein levels in RA synovial tissues. Drawing from bioinformatic insights and empirical data, we deduced that TIMP1 is implicated in rheumatoid pathogenesis, aligning with prior studies that reported elevated TIMP1 in the serum of RA patients, correlating with disease activity [32,33]. Few studies have examined the its expression in synovial tissues. And we confirmed that TIMP1 was upregulated in RA synovial tissues and also elevated in FLS, corroborating its cytokine-like profile. TIMP1, known for its anti-proteolytic properties, also function as a cytokine function and directly influences the inflammatory process [25]. TIMP1 is elevated in the plasma of patients with a variety of inflammatory conditions, including RA [34,35]. Specific macrophage and T cell subsets have exhibited express TIMP1 expression in response to inflammation [36,37]. While TIMP1 was moderately upregulated in macrophages, its expression in T cell subsets was comparatively subdued. We hypothesize that in the peripheral synovial tissues of early-stage RA patients, TIMP1 might function as a proinflammatory cytokine, being secreted predominantly by macrophages and activated effector adaptive immune cells.

Elevated concentrations of TIMP1 have been observed in synovial fluid, indicating a clear association between RA synovial tissues and TIMP1 [38]. Through the WGCNA algorithm, TIMP1 emerged within the brown module, which was further enriched for function like immune receptor activity, cytokine activity, protein tyrosine kinase activity, SH2 domain binding, NAD + nucleosidase activity, microtubule binding, and lipopeptide binding. A myriad of studies have demonstrated the interconnectedness of cell ferroptosis, inflammation, and the pivotal role of immune cells. Thus, the heightened activity of immune receptors, cytokines, and pertinent receptors is thus expected. Adaptor proteins, which aid in the signal transduction of receptor tyrosine kinase, typically contain SH2 domains. Studies have confirmed that receptor tyrosine kinase is activated by inflammatory signaling, resulting in heightened sensitivity to ferroptosis [39,40]. As essential cellular redox systems, NAD(P)H induces oxidative injury to cellular membranes [41]. Microtubule accumulation of iron in senescent cells caused by impaired ferritinophagy [42] has been confirmed. Thus, the function of brown module genes is likely tied to the pathological process of ferroptosis in synovial tissues of RA.

Numerous studies have confirmed the ferroptosis of FLS in RA. Wu et al. emphasized the sensitivity of FLS to ferroptosis, noting and its increased presence in RA patients' synovial fluid, correlating with disease activity [43]. In addition, some evidence suggests TIMP1's roles in ferroptosis. TIMP1 was elevated in a cigarette smoke extract-induced ferroptosis model that was rescued by an inhibitor of ferroptosis [44]. The disruption of TIMP1 in cardiac microvascular endothelial cells (CMECs) led to the activation of TFR-1 and the subsequent ferroptosis of CMECs [45]. We propose that TIMP-1 plays a "bridge" role in exceptionally large molecular interaction networks. Following the initiation of iron-dependent cell death, TIMP1 ascends and amplifies the cascade effect on
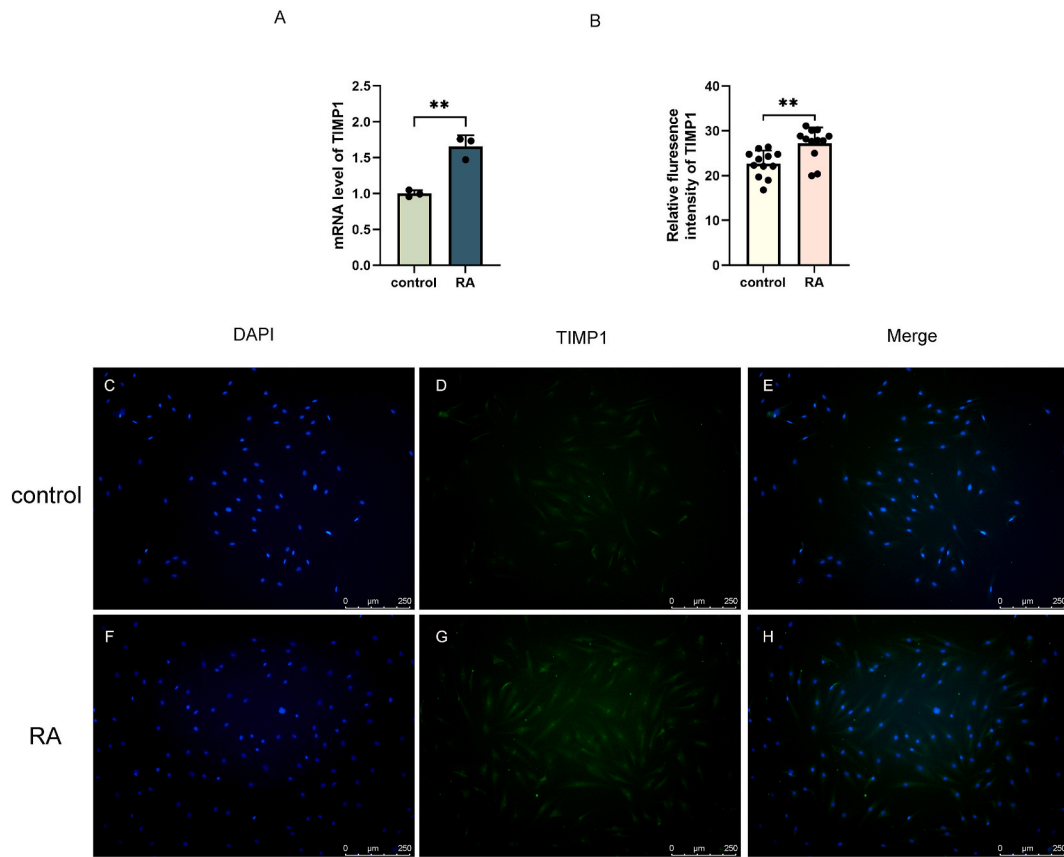
Fig. 12. RT–qPCR and immunofluorescence analysis of FLS. (A) RT–qPCR analysis of TIMP1 mRNA in the control and RA groups. (B) Quantitative analysis of immunofluorescence stainings between groups. **p < 0.01 compared with the control group. (C) Green signals denote TIMP1 proteins and blue signals denote nuclei. (For interpretation of the references to color in this figure legend, the reader is referred to the Web version of this article.)
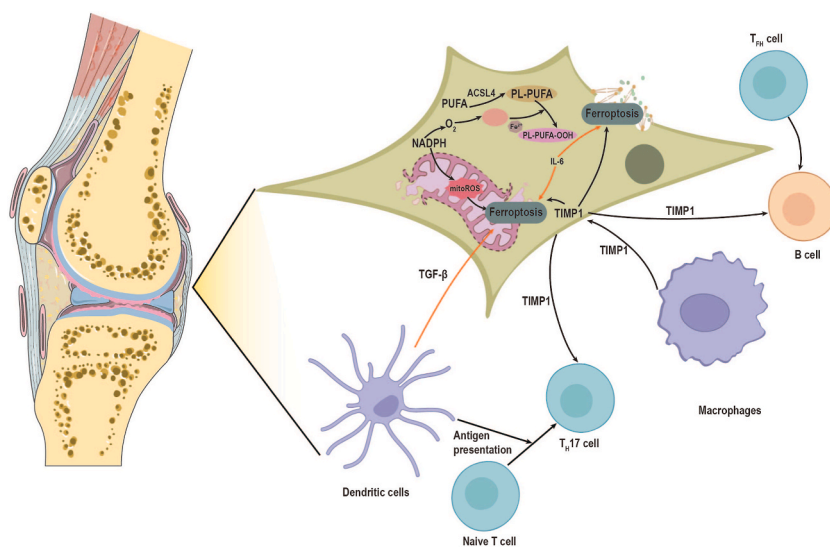

Fig. 13. Proposed mechanism of TIMP-1 role in ferroptosis. This figure illustrates a potential mechanism based on hypotheses and theoretical conjectures from the current study, which has not yet been experimentally validated.

downstream cells, most likely through classical cytokines (Fig. 13).

This study had certain limitations, specifically the inclusion of relatively small validation samples. Future research should aim to augment the sample size and conduct cohort studies in order to corroborate our findings. The study explored the changes in ferroptosis in RA peripheral synovial tissue, yet the specific mechanisms of action require further clarification. Furthermore, it is imperative that these results be validated through clinical trials.

5. Conclusions

This study delved into the role of ferroptosis in the pathophysiology of peripheral immune tolerance deficiency in RA synovial tissues, providing novel insights into the underlying mechanisms. The dysregulation of TIMP1, a ferroptosis-related gene, was observed in RA patients and may serve as a potential biomarker and therapeutic target.

Funding

Institutional review board statement

The human samples and experimental procedures were approved by the Shenzhen Hospital of Peking University and conducted in accordance with their accredited ethical guidelines (2020–007).

Data availability statement

Data will be made available on request. The data used in bioinformatic analysis were obtained from the public database GEO database (https://www.ncbi.nlm.nih.gov/geo/) and ImmPort (https://www.immport.org/shared/study/SDY998).

CRediT authorship contribution statement

Hongli Wang: Writing – original draft, Software, Methodology, Investigation, Formal analysis, Conceptualization. **Miaomiao Zhang:** Visualization, Formal analysis, Data curation. **Yiping Hu:** Resources. **Juan He:** Supervision, Conceptualization. **Yuchao Zhong:** Writing – review & editing, Visualization, Validation, Supervision. **Yong Dai:** Supervision, Data curation, Conceptualization. **Qingwen Wang:** Writing – review & editing, Writing – original draft, Visualization, Supervision, Resources, Conceptualization.

Declaration of competing interest

The authors declare that they have no known competing financial interests or personal relationships that could have appeared to influence the work reported in this paper.

Appendix A. Supplementary data

Supplementary data to this article can be found online at https://doi.org/10.1016/j.heliyon.2024.e33648.

References

[1] S. Alivernini, G.S. Firestein, I.B. McInnes, The pathogenesis of rheumatoid arthritis, Immunity 55 (12) (2022) 2255–2270.
[2] G.J. Tobón, P. Youinou, A. Saraux, The environment, geo-epidemiology, and autoimmune disease: rheumatoid arthritis, Autoimmun. Rev. 9 (5) (2010) A288–A292.
[3] N. Komatsu, H. Takayanagi, Mechanisms of joint destruction in rheumatoid arthritis - immune cell-fibroblast-bone interactions, Nat. Rev. Rheumatol. 18 (7) (2022) 415–429.
[4] J.S. Smolen, et al., Rheumatoid arthritis, Nat. Rev. Dis. Prim. 4 (2018) 18001.
[5] S.J. Dixon, et al., Ferroptosis: an iron-dependent form of nonapoptotic cell death, Cell 149 (5) (2012) 1060–1072.
[6] H.F. Yan, et al., Ferroptosis: mechanisms and links with diseases, Signal Transduct. Targeted Ther. 6 (1) (2021) 49.
[7] Y. Xie, et al., Ferroptosis: process and function, Cell Death Differ. 23 (3) (2016) 369–379.
[8] C.M. Bebber, et al., Ferroptosis in cancer cell Biology, Cancers 12 (1) (2020).
[9] G.B. Senator, K.D. Muirden, Concentration of iron in synovial membrane, synovial fluid, and serum in rheumatoid arthritis and other joint diseases, Ann. Rheum. Dis. 27 (1) (1968) 49–54.
[10] L.F. van Vulpen, et al., The detrimental effects of iron on the joint: a comparison between haemochromatosis and haemophilia, J. Clin. Pathol. 68 (8) (2015) 592–600.

[11] J.F. Telfer, J.H. Brock, Proinflammatory cytokines increase iron uptake into human monocytes and synovial fibroblasts from patients with rheumatoid arthritis, Med Sci Monit 10 (4) (2004) Br91–B95.

[12] Z. Xie, et al., ROS-dependent lipid peroxidation and Reliant Antioxidant ferroptosis-Suppressor-protein 1 in rheumatoid arthritis: a Covert clue for potential therapy, Inflammation 44 (1) (2021) 35–47.

[13] H.B. Ferreira, et al., Insights in the role of lipids, oxidative stress and inflammation in rheumatoid arthritis unveiled by new trends in lipidomic investigations, Antioxidants 10 (1) (2021).

[14] C.M. Quiñonez-Flores, et al., Oxidative stress relevance in the pathogenesis of the rheumatoid arthritis: a systematic review, BioMed Res. Int. 2016 (2016) 6097417.

[15] U. Fearon, et al., Hypoxia, mitochondrial dysfunction and synovial invasiveness in rheumatoid arthritis, Nat. Rev. Rheumatol. 12 (7) (2016) 385–397.

[16] M.E. Ritchie, et al., Limma powers differential expression analyses for RNA-sequencing and microarray studies, Nucleic Acids Res. 43 (7) (2015) e47.

[17] N. Zhou, J. Bao, FerrDb: a manually curated resource for regulators and markers of ferroptosis and ferroptosis-disease associations, Database (2020) 2020.

[18] P. Bardou, et al., jvenn: an interactive Venn diagram viewer, BMC Bioinf. 15 (1) (2014) 293.

[19] P. Langfelder, S. Horvath, WGCNA: an R package for weighted correlation network analysis, BMC Bioinf. 9 (2008) 559.

[20] D. Aran, Z. Hu, A.J. Butte, xCell: digitally portraying the tissue cellular heterogeneity landscape, Genome Biol. 18 (1) (2017) 220.

[21] Y. Hao, et al., Integrated analysis of multimodal single-cell data, Cell 184 (13) (2021) 3573–3587.e29.

[22] M.B. Buechler, et al., Cross-tissue organization of the fibroblast lineage, Nature 593 (7860) (2021) 575–579.

[23] Z. Fang, et al., C-reactive protein promotes the activation of fibroblast-like synoviocytes from patients with rheumatoid arthritis, Front. Immunol. 11 (2020) 958.

[24] J. Chen, et al., Berberine chloride suppresses non-small cell lung cancer by deregulating Sin3A/TOP2B pathway in vitro and in vivo, Cancer Chemother. Pharmacol. 86 (1) (2020) 151–161.

[25] B. Schoeps, et al., Identification of invariant chain CD74 as a functional receptor of tissue inhibitor of metalloproteinases-1 (TIMP-1), J. Biol. Chem. 297 (3) (2021) 101072.

[26] I.B. McInnes, G. Schett, Pathogenetic insights from the treatment of rheumatoid arthritis, Lancet 389 (10086) (2017) 2328–2337.

[27] D. Venkatesh, et al., MDM2 and MDMX promote ferroptosis by PPARα-mediated lipid remodeling, Genes Dev. 34 (7–8) (2020) 526–543.

[28] Y. Chen, et al., The interaction between ferroptosis and inflammatory signaling pathways, Cell Death Dis. 14 (3) (2023) 205.

[29] H. Luo, R. Zhang, Icariin enhances cell survival in lipopolysaccharide-induced synoviocytes by suppressing ferroptosis via the Xc-/GPX4 axis, Exp. Ther. Med. 21 (1) (2021) 72.

[30] L.F. van Vulpen, et al., IL-1β, in contrast to TNFα, is pivotal in blood-induced cartilage damage and is a potential target for therapy, Blood 126 (19) (2015) 2239–2246.

[31] S.Z. Hassan, et al., Oxidative stress in systemic lupus erythematosus and rheumatoid arthritis patients: relationship to disease manifestations and activity, Int J Rheum Dis 14 (4) (2011) 325–331.

[32] Z.Z. Wang, et al., [Significance of serum MMP-3, TIMP-1, and monocyte CD147 in rheumatoid arthritis patients of damp-heat Bi-syndrome and of cold-damp Bi-syndrome], Zhongguo Zhong Xi Yi Jie He Za Zhi 33 (6) (2013) 770–773.

[33] P.A. Klimiuk, et al., Regulation of serum matrix metalloproteinases and tissue inhibitor of metalloproteinases-1 following rituximab therapy in patients with rheumatoid arthritis refractory to anti-tumor necrosis factor blockers, Rheumatol. Int. 35 (4) (2015) 749–755.

[34] D.M. Cortez, et al., IL-17 stimulates MMP-1 expression in primary human cardiac fibroblasts via p38 MAPK- and ERK1/2-dependent C/EBP-beta , NF-kappaB, and AP-1 activation, Am. J. Physiol. Heart Circ. Physiol. 293 (6) (2007) H3356–H3365.

[35] E. Roeb, et al., Regulation of tissue inhibitor of metalloproteinases-1 gene expression by cytokines and dexamethasone in rat hepatocyte primary cultures, Hepatology 18 (6) (1993) 1437–1442.

[36] C. Roma-Lavisse, et al., M1 and M2 macrophage proteolytic and angiogenic profile analysis in atherosclerotic patients reveals a distinctive profile in type 2 diabetes, Diab Vasc Dis Res 12 (4) (2015) 279–289.

[37] A. Adamson, et al., Tissue inhibitor of metalloproteinase 1 is preferentially expressed in Th1 and Th17 T-helper cell subsets and is a direct STAT target gene, PLoS One 8 (3) (2013) e59367.

[38] G. Giannelli, et al., MMP-2, MMP-9, TIMP-1 and TIMP-2 levels in patients with rheumatoid arthritis and psoriatic arthritis, Clin. Exp. Rheumatol. 22 (3) (2004) 335–338.

[39] G. Koytiger, et al., Phosphotyrosine signaling proteins that drive oncogenesis tend to be highly interconnected, Mol. Cell. Proteomics 12 (5) (2013) 1204–1213.

[40] J. Tsoi, et al., Multi-stage differentiation defines melanoma subtypes with differential vulnerability to drug-induced iron-dependent oxidative stress, Cancer Cell 33 (5) (2018) 890–904.e5.

[41] J. Zheng, M. Conrad, The metabolic underpinnings of ferroptosis, Cell Metab 32 (6) (2020) 920–937.

[42] S. Masaldan, et al., Iron accumulation in senescent cells is coupled with impaired ferritinophagy and inhibition of ferroptosis, Redox Biol. 14 (2018) 100–115.

[43] J. Wu, et al., TNF antagonist sensitizes synovial fibroblasts to ferroptotic cell death in collagen-induced arthritis mouse models, Nat. Commun. 13 (1) (2022) 676.

[44] A. Sampilvanjil, et al., Cigarette smoke extract induces ferroptosis in vascular smooth muscle cells, Am. J. Physiol. Heart Circ. Physiol. 318 (3) (2020) H508–h518.

[45] P. Shi, et al., Neutrophil-like cell membrane-coated siRNA of lncRNA AABR07017145.1 therapy for cardiac hypertrophy via inhibiting ferroptosis of CMECs, Mol. Ther. Nucleic Acids 27 (2022) 16–36.